Planar photonic chips with tailored angular transmission for high-contrast-imaging devices

Yan Kuai
Department of Optics and Optical Engineering, Institute of Photonics, University of Science and Technology of China, Number 96 Jinzhai Road, Hefei, Anhui 230026 https://orcid.org/0000-0002-0647-7913

Junxue Chen
Guilin University of Technology https://orcid.org/0000-0002-1104-627X

Gang Zou
University of Science and Technology of China https://orcid.org/0000-0002-5041-5242

Joseph Lakowicz
Univ. Maryland

Douguo Zhang (dgzhang@ustc.edu.cn)
University of Science and Technology of China https://orcid.org/0000-0003-1230-8742

Article

Keywords: microscopy, total internal reflection, photonics

Posted Date: July 26th, 2021

DOI: https://doi.org/10.21203/rs.3.rs-646324/v1

Version of Record: A version of this preprint was published at Nature Communications on November 25th, 2021. See the published version at https://doi.org/10.1038/s41467-021-27231-6.

Abstract

A limitation of standard brightfield microscopy is its low contrast images, especially for thin specimens of weak absorption, and biological species with refractive indices very close in value to that of their surroundings. Here, we demonstrate, using a planar photonic chip with tailored angular transmission as the sample substrate, a standard brightfield microscopy can provide both darkfield and total internal reflection (TIR) microscopy images with one experimental configuration. The image contrast is enhanced without altering the specimens and the microscope configurations. This planar chip consists of several multilayer sections with designed photonic band gaps and a central region with dielectric nanoparticles, which does not require top-down nanofabrication and can be fabricated in a large scale. The photonic chip eliminates the need for a bulky condenser or special objective to realize darkfield or TIR illumination. Thus, it can work as a miniaturized high-contrast-imaging device for the developments of versatile and compact microscopes.

Introduction

Modern microscopes can produce images of high resolution and high magnifications[1, 2, 3]. Enough contrast of the image is also essential to clearly reveal the details of the specimens[4, 5], resulting in the widespread use of fluorescent probes. A variety of techniques have been developed to improve image contrast without modification of the samples (label-free imaging). One approach is darkfield illumination, which is particularly suitable for specimens that display little or no absorption and/or weakly absorbing biological samples. Darkfield microscopy (DFM) has been widely used in many fields of science and engineering, such as biological imaging, nanoparticle characterization and inspection of semiconductor devices [6, 7, 8, 9]. However, it cannot be a simple and inexpensive imaging system. In a typical DFM, firstly, the specimen is illuminated at oblique angles far from the direction normal to the sample, then a bulky darkfield condenser is needed. Secondly, only light that is scattered by the specimen into a cone of apex angle cantered around the microscope's optical axis should be collected. To meet this requirement, the objective is chosen such that it collects rays over a small range of angles which are far from the normal axis, so no light directly from the darkfield condenser contributes to the image. The regions on the specimen where there are no small features to scatter light are almost completely dark, often resulting in high-contrast images and giving 'darkfield' microscopy its name. Thirdly, the specialized condenser, objective and additional components are prone to misalignment and add cost and complexity to the microscope [10, 11]. The use of a bulky condenser also results in the very small illumination area (of micrometer scale).

In recent years, there has been interesting in developments of new imaging instruments with the nanophotonic devices to downsize or simplify the microscope setup and improve the imaging performances. For example, two multifunctional and compact metasurface layers were used to develop a compact phase gradient microscope, which can generate a quantitative phase gradient image with increased image contrast[12]. The combination of ptychographic coherent diffractive imaging with sub-

surface nanoaperture arrays was shown to yield an enhancement of both the reconstructed phase and amplitude[13]. A luminescent photonic substrate with a controlled angular fluorescence emission profile was used in a conventional microscopy to replace the bulk condenser for miniaturized lab-on-chip darkfield imaging devices [14, 15].

Here, we demonstrate that after the attaching of a planar photonic chip to the substrate of a standard brightfield microscopy (BFM), both darkfield and total internal reflection (TIR) imaging can be realized in one experimental setup without the use of a bulky darkfield condenser and other specialized components. The new microscopes can be named as chip-based darkfield microscopy (C-DFM) and chip-based total internal reflection microscopy (C-TIRM). The C-DFM and C-TIRM have the merits of large illumination area, high imaging contrast, simple configuration and easy for optical-alignment. Both DFM and TIRM emphasize the high-spatial-frequency components associated with small features in the specimen morphology and in some imaging scenarios, it can even provide resolution beyond the diffraction limit[16, 17]. Different from the DFM that uses far-field propagating light as the illumination source, the TIRM uses pure evanescent waves on the surface as the illumination source, which will have higher spatial frequency and are more sensitive to the changes on the surface. It is ideally suited to analyze the localization and dynamics of molecules and events occurring near the interface, such as the plasma membrane.

Results

Configuration of the planar photonic chip. The proposed chip is designed to provide evanescent wave excitation (or TIR) at 640 nm wavelength and darkfield conditions at 750 nm wavelength, using a standard brightfield microscope. The photonic chip consists of three parts (Figure 1a). The middle is a dielectric layer (thickness about 2 μm) doped with TiO2 nanoparticles (diameter at 60 nm). The bottom and top are the dielectric multilayers with different PBGs[18, 19]. The multilayers are made of alternating SiO_2 and SiN_x layers. Details of the structural parameters are given in Figure S1. The color-scale encoded reflectivity (Figure 1b and 1c) of the bottom and top multilayer was calculated by using transfer matrix method (TMM)[20].

For the bottom multilayer, when the incident beams are of transverse-magnetic (TM) or transverse-electric (TE) polarization, there are reflection valleys at nearly 0^o (Figure 1d), meaning that only a near-normal incident beam can transmit through this multilayer (inset of Figure 1d). The unusual transmission of the bottom multilayer layer is the result of two periodical dielectric structures, separated by a thicker layer of SiO_2 (Figure S1). Surface normal transmission occurs at designed wavelengths (640 and 750 nm here) and no transmission happens at other angles for the designed wavelengths (Figure S2). This restricted surface-normal transmission prevents the scattered light from leaving the bottom layer.

When the transmitted beam reaches the middle layer containing TiO_2 nanoparticles, its propagating direction will be changed due to the scattering at the nanoparticles. A portion of the scattering lights

return to the bottom multilayer, but they will bounce back to the scattering layer due to the PBG of the bottom multilayer, and only scattering light at near normal angle can escape through the bottom multilayer. Some of the scattered light will reach the top multilayer. The PBG of top multilayer was designed (Figure 1c) so that the scattering light at 750 nm wavelength can transmit at designed polar angles (from 27^o to 42 ^{o} in glass, within N.A < 0.7, the reflection valleys on Figure 1e, TM-polarization). For the scattering light with propagating directions within N.A <0.7, it will be reflected to the scattering layer, and then reflected by the bottom multilayer. When the N. A of the imaging objective is less than 0.7, darkfield imaging can be realized[1, 21]. For the scattering light at 640 nm wavelength, it lies in the forbidden band (Figure 1c). When the scattering angle is larger than the critical angle, TIR and evanescent waves will happen at the multilayer/air interface, resulting in TIR imaging[11] .

In brief, the scattering layer is to provide light of various propagating directions. The role of the top multilayer is to select the transmitting angles of the scattered light, either larger than a designed polar angle or induced evanescent waves on the top-surface. The bottom multilayer only allows the transmittance of near-normal incident beam, so it can recycle scattering light into propagation angle ranges that are transmitted by the top multilayer, and then amplify the light intensity on or out of the top multilayer. Through properly design of the PBGs, the desired angular transmission of the photonic chip (bottom and top multilayer) can be realized, which is benefit for high contrast imaging.

Fabrication and characterization of the planar photonic chip.

The multilayers were fabricated via plasma-enhanced chemical vapour deposition (PECVD) and characterized with a scanning electron microscope (SEM, Figure 2a and 2b). The manufacturing procedures are described in Figure S3 and section methods. The color-scale encoded reflectivity of the bottom and top dielectric multilayer were measured with a reflection back focal plane (R-BFP) imaging setup [22, 23] (Figure S4-S6) respectively, as shown in Figure 2c and 2d, which are nearly consistent with numerical calculations (Figure 1b and 1c) and experimentally verify the desired roles of two multilayers.

In the imaging experiments, two low-coherent light-emitting diodes (LED) were used to generate the scattering lights from the non-fluorescent TiO_2 nanoparticles, which will work as the illumination source for the darkfield image at 750 nm wavelength or TIR images at 640 nm wavelength. Compared to the use of a laser light source for label-free imaging, the LED light will greatly reduce the speckles or interference noise on the optical images. On the other hand, a renewed interest in transmitted darkfield microscopy has arisen due to its advantage when used in combination with fluorescence microscopy. Compared to fluorescence emission from quantum dots (QDs) for the illumination source in luminescent-surface-based darkfield imaging[14], the scattered light originating from the high-intensity LED light can excite fluorophores more efficiently than the fluorescence-light from QDs. Also, the LED light source will not encounter the problem of photobleaching or blinking that is typical for QDs and other fluorophores, then the proposed C-DFM and C-TIRM will be more stable.

The transmission BFP images of whole photonic chip were measured with the experimental setup (Figure 3a), which presents the transmission directions of the scattered light from the TiO2 nanoparticles. Figure 3 demonstrates three predicted phenomena. Firstly, each point on the BFP image represents one emitting angle (both polar and azimuthal angle) of the scattering light, so the intensity distribution on the BFP images can represent the propagating directions of the scattered light passing through the top multilayer [23]. Secondly, comparisons between the top and bottom BPF images on Figure 3d and 3f, show that the use of the bottom multilayer can highly amplify the intensity of the scattered light that reaches the top multilayer. Thus, it results in much more intense light exiting from the top multilayer at the designed polar angles, and more intense evanescent waves, which benefit both darkfield and TIR imaging. Thirdly, the intensity of the scattered light within N. A< 0.70 and that with N.A from 0.70 to 1.49 were derived from Figure 3d and Figure 3f, as shown in Figure 3e and Figure 3g. It is clearly show that this chip can efficiently prevent the direct transmission at lower N.A (corresponding to small polar angle), and most of transmission energy (about 98.5%) was localized inside the large N.A regions (0.7-1.49), which is favorable for the contrast of DFM or TIRM images.

The planar photonic chip working as a high-contrast imaging device. In the following experiments, a polymer nanowire and polymer microwire were used as the specimens, although they can certainly be replaced with real cells. The nanowire is approximately 70 nm in diameter, and the microwire is approximately 3 to 4 μm in diameter (Figure S7b). The single polymeric nanowire was located on a polymeric microwire that are both placed on a coverslip. A regular air objective (60 X, N.A 0.70) was used for the standard brightfield imaging under the normal illumination of LED light at 640 and 750 nm wavelengths, and the brightfield images are shown in Figure 4b and 4f. Secondly, When the photonic chip was attached below this coverslip with index-matched oil, C-DFM and C-TIRM images of the polymer wires are much more defined. When the illumination wavelength was 750 nm, the scattered light from the chip will be out of the N.A of the objective. The images (Figure 4c and 4d) show typical darkfield characters, a bright image of the specimens superimposed onto a dark background. The darkfield image contrast (CR), calculated as the difference between the maximum and minimum image intensity values divided by their sum (Figure 4e and 4i), was significantly improved when comparing with that of the brightfield image (Figure 4e). The polymer wires on Figure 4d is brighter than those on Figure 4c, verifying that the bottom multilayer can recycle the scattering light and amplify the intensity of the scattered light that transmit through the top multilayer at the designed polar angles, which are consistent with the transmission BFP images (Figure 3d and 3f).

Except for the differences in contrasts, the darkfield images of the nanowire appear discontinuous when it crosses the microwire. This phenomenon can be explained as following. When the illumination wavelength is 750 nm, the specimen will be illuminated not only by the transmitting light at oblique polar angles (0. 70 <N.A <1.0) and at all azimuths, but also evanescent waves (N. A >1.0) on the coverslip-air interface induced by the TIR, as shown in Figure 3d. In this crossing area, the nanowire is on the microwire and is far away from the coverslip. Due to the longitudinal decay of evanescent waves [24], this crossed section will not be imaged. On the contrary, this longitudinal air gap cannot be discovered from

brightfield images (Figure 4b and 4f). This phenomenon will be more obviously, as that the nanowire is nearly invisible in the crossing area, when the wavelength was changed to 640 nm (Figure 4g and 4h). In this case, the specimens are illuminated only by pure evanescent waves, and the BFM was transformed to a C-TIRM with the aid of this photonic chip as an add-on.

When the polymer wires were replaced with polymer particles, the images enhancement induced by the photonic chip is also obvious (Figure S8). The edge of the microparticles is shaper on the TIR image (Figure S7c) than that on the darkfield image (Figure S7b), because that the TIR imaging uses higher-spatial-frequency component of the illumination source and can provide higher spatial resolution. It should be noted that the photonic chip still works when the specimens were immersed in water solution (Figure S9). The phenomena on Figure 4f-4i verify that, using this high compatible photonic chip below the substrate, the TIRM images can be captured by a standard BFM, which can focus on the targets within the evanescent field (100 to 200 nm) only, rather than those contained in the entire sample.

Excitation of large-scale surface plasmons with the planar photonic chip. Furthermore, it can be anticipated that this photonic chip has the potentials to excite other kinds of surface waves under normal incidence, such as surface plasmons (SPs) and Bloch surface waves (BSWs) that are more sensitive to environmental changes than the evanescent waves used in TIR fluorescence microscopy[25]. Typically, either a bulk prism, or a nanofabricated structure, or an oil-immersed objective is required for the excitation of SP or BSWs, which result in either bulk and complicated system or limited excitation areas[26]. However, these limitations can be removed by using the photonic chip. To verify this point, the top multilayer was replaced with a coverslip coated with a 55-nm-thick Ag film (Figure 5a). The images (Figure 5b) show a typical character of surface-sensitive patterns with enhanced imaging contrast (Figure 5d), where the nanowire appears discontinuous in the cross-region with the microwire. The phenomena verify the excitation of the SPs. The advantage of images illuminated by SPs over the brightfield images will be obviously when the diameter of the polymer nanoparticles changes from 200 nm to 50 nm (from Figure 5e to 5f). When the diameter of the polymer nanoparticles is about 50 nm, these nanoparticles are nearly invisible on the brightfield image (Figure 5f), but are visible on the image illuminated by the SPs (Figure 5e). The excitation of the SPs with the normal incident light will make the optical path easily aligned and simplify the configuration. The use of a planar chip means that the excitation areas of the SPs can be much larger than that excited with in-plane nanostructures (such as the inscribed gratings), which is favorable for high throughput imaging, sensing and tracking of the specimens.

Discussion

In summary, through placing a photonic chip below the specimens, a standard BFM can be easily transformed to both a C-DFM and C-TIRM without modifying the configuration or the specimens. The principle lies on that, under normal incidence, both the inverted hollow cones of light and various evanescent waves can be generated with this photonic chip due to its tailored angular transmission. The roles of this photonic chip working as a high contrast imaging device, are confirmed by both theoretical and experimental results. Thus, it demonstrates the potential of the proposed imaging device for a novel

type of versatile and compact microscopy. The working wavelengths of the photonic chip can be tuned through changing thickness and refractive index of the dielectric layers; thus, the devices enable multispectral darkfield and TIR imaging using simple brightfield microscopes[14]. If the specimens are fluorescent, fluorescence imaging also can be realized, similar as the TIRF [27]. Then, the setup can perform simultaneous C-DFM/C-TIRM and fluorescence microscopy of the same specimen, and thus make it possible to combine the strengths of both labelled and label-free detection and fluorescent imaging technologies in one integrated set-up [28, 29, 30]. When combining with stochastic optical reconstruction technique, the C-TIRM will has the potential to be a chip-based wide field-of-view nanoscopy [2]. The imaging device can be washed, sterilized and used multiple times. It has proved affordable and easy for users to launch as an add-on to a regular brightfield microscope, thus, it will make full use of the BFM that can be found in many academic and industrial labs.

When comparing with bulk Abbe condensers used in a conventional DFM, and prism or oil-immersed objective used in conventional TIR imaging, this imaging device made of planar chip is more compact, low cost and easy aligned. It can be fabricated on an extremely large substrate with standard deposition and spin-coating method, without any top-down nanofabrication procedures, thus open new avenues towards the design of a fully integrated on-chip microscopy. Different from the condenser or objective that has limited illumination area (of micrometer scale), this imaging device enables extremely large illumination area up to centimeter-scale or even larger. In the future, the combination of photonic chip with micro lens arrays for light collection have the potential for extraordinarily high throughput, with illumination and collection done in parallel over large areas, completely removing the dependency on a bulky objective lens [3].

Methods

Fabrication of the planar phonic chips working as the compact imaging-devices. The top and bottom dielectric multilayers were fabricated via PECVD (Oxford System 100) of SiO_2 and SiN_x on a coverslip (0.17 mm thickness) at a vacuum 0.1 m torr and temperature of 300 ^{o} C. Before the PECVD of a dielectric multilayer, the coverslip was cleaned with piranha solution and then with nanopure deionized water and dried with an N_2 stream. The process of PECVD depends on the chemical reaction of SiH4 with N_2O and NH_3 at high temperature. The refractive index of SiN_x can be adjusted from 1.9 to 2.4 by changing the ratio of SiH_4 to NH3. The SiO_2 layer is of the low (L) refractive index dielectric and the SiN_4 layer is the high (H) one. Thickness of each layer was presented in details in Figure S1. There are 18 pairs of SiN_x (2) + SiN_x (3) and 11 pairs of SiO_2 + SiNx (1) in total for the bottom multilayer. There are 10 pairs of SiO_2 + SiN_x (1) in total for the top multilayer. The top and bottom multilayer were fabricated on two independent coverslips for the BFP imaging experiments to measure the PBG of the multilayer (Figure 2 and Figure 3).

The spacer layer between the top and bottom multilayer is made of Intermediate Coating IC1-200, which is a polysiloxane-based spin-on dielectric material. The IC1-200 solution doped with TiO_2 nanoparticles

(diameter at about 60 nm) was then spin-coated on to the bottom multilayer, which will work as the scattering layer to generate scattering light of various propagating directions. Thickness of the spacer layer is about 2 μm and its refractive index is about 1.41. The SEM image of the scattering nanoparticle TiO_2 was shown in Figure S7a.

For the darkfield and TIR imaging experiments, the three parts of the planar photonic chip will be assembled together with the refractive index matched oil and then form the unit substrate (Figure 4a). The silver film was deposited on the bare coverslip with the thermal evaporation method, whose thickness is about 55 nm. For the surface-imaging with SPs (Figure 5), this coverslip coated with Ag film was attached onto the spacer (scattering) layer with refractive index matched oil.

It should be noted, this photonic chip still can be used to realize the darkfield and TIR imaging if the bottom multilayer was removed, as shown Figure 4c and Figure 4g. However, the obtained darkfield and TIR images will be much weaker than those (Figure 4d and Figure 4h) obtained with the whole photonic chip (Top multilayer+ scattering layer + bottom multilayer). Or in other word, the bottom multilayer can recycle scattering light into propagation angle ranges that are transmitted by the top multilayer, and then amplify the light intensity on or out of the top multilayer, which was verified by the comparisons between the top and bottom images on Figure 3d and Figure 3f.

Preparation of the polymer wires and nanoparticles as the specimens to be imaged. The typical procedure for the fabrication of electro spun micro and nano fibers is given below. A 2 ml formic solution (solvent for the Nylon) containing 1.6 g Nylon 6 was ejected at a continuous rate using a syringe pump through a stainless-steel needle. A voltage of 10 kV was applied to the needle with a high voltage power supply and a feed rate of 0.2 mm per minute was maintained with a syringe pump. A collector (the glass substrate with the fabricated dielectric multilayer) was placed at 10 cm from the needle tip to collect the polymer nanowires. By replacing the solution in the syringe pump into a tetrahydrofuran solution containing 0.25g hydrogel, the hydrogel microwire can be produced with the same procedure. The SEM images of the polymer wires are shown in Figure S7.

The polystyrene nanoparticles (Figure 5, Figure S8) were purchased from Thermo Fisher Scientific (USA). The certified mean diameters of the nanoparticles supplied were about 20 nm, 50 nm, 100 nm, 200 nm and 2μm. The SEM images of these nanoparticles are shown in Figure S7. The nanoparticles dispersed in water are spin coated on the substrate. After dried by hot plate, the nanoparticles are fixed on the surface of the substrate.

In the darkfield and TIR imaging (Figure 4, Figure S8 and S9), the polymer wires and polystyrene nanoparticles were placed on a clean coverslip, which was then attached to the top surface of the photonic chip (Figure 1a, Figure 4a) with refractive index matched oil between them. However, the specimens (wires and particles) can also be put on the top surface of the photonic chip directly for darkfield and TIR imaging, then this planar photonic chip both holds and illuminates the specimen. In the

brightfield imaging used for comparisons, this photonic chip was removed. For the surface-imaging with SPs (Figure 5), the wires and nanoparticles were placed on the silver film directly.

Optical characterization set-up. All optical measurements were performed on modified optical microscope (Nikon Ti2-U). For the reflection BFP imaging setup (Figure S4), an oil immersion objective (CFI Apochromat TIRF 100X, N.A. 1.49, W.D. 0.12mm) from Nikon, Japan was used to fully measure the reflecting angular distribution, which corresponds to the polar angle ranging from -80^o to 80^o in the oil medium. To minimize the interference fringes on the BFP images, we used a noncoherent light (tungsten bromine lamp combined with a serials of band-pass filters) as the illumination source. The center wavelengths of the band pass filter ranges from 600 nm to 790 nm (20 filters in-total), with a full width at half maximum (FWHM) of 10±2nm. The Neo sCMOS detector for recording the BFP images was from Andor Oxford Instruments (UK). By properly tuning the distance between the tube lens and the detector, BFP image of the objective can be recorded. At each incident wavelength, one BFP image can be obtained. From all these BFP images (Figure S4, Figure S5 and Figure S6), PBGs of the top and bottom multilayers can be derived.

For the transmitted BFP images (Figure 3a), the illumination source was changed to LED with center wavelength at 640 and 750 nm. Two bandpass filters (full width at half maximum (FWHM) of 10 ±2 nm, center wavelengths of 640 and 750 nm, Thorlabs Inc.) were used to select the required emission wavelengths from the LED sources. Under normal incidence, the transmitting angular distribution of the scattering light escaping out of the photonic chip was measured with the same objective with N.A at 1.49. The detector and tube lens are the same as those used in reflection BFP imaging setup. It should be noted, in the BFP imaging of the photonic chip and independent multilayer, no specimens (polymer wires and polystyrene particles) were put on the chip.

In the darkfield and TIR imaging of the specimens, a regular air objective (CFI Super Plan Fluor ELWD 60X, N.A. 0.70, W.D. 2.61-1.79mm) was used. The distance between the tube lens and the detector was changed so that the front focal plane (FFP) of the objective can be imaged. The LED with bandpass filter was used as the illumination source.

Declarations

Data availability. The data that support the plots within this paper and other finding of this study are available from the corresponding author upon reasonable request.

Acknowledgements. This work was supported by the Ministry of Science and Technology of China (grant no. 2016YFA0200601), the National Nature Science Foundation of China (grant no. 11774330, U20A20216), the Anhui Initiative in Quantum Information Technologies (grant no. AHY090000). J. R. Lakowicz thanks the National Institute of General Medical Sciences for support under grant nos. R01 GM125976 and R21 GM129561 and the National Institutes of Health for support under grant nos. S10OD19975 and S10RR026370. The work was partially carried out at the University of Science and

Technology of China's Center for Micro and Nanoscale Research and Fabrication. D.G.Z is supported by a USTC Tang Scholarship and the Advanced Laser Technology Laboratory of Anhui Province (grant no. 20192301).

Author contributions. D.G.Z. initiated the work, supervised the project and drafted the manuscript. Y.K. and D.G.Z carried out the optical experiments and fabricated the samples, Y.K, and J.X. Chen carried out the theoretical calculations. G.Z. contributed to the fabrications of polymer wires. J.R.L. assisted in writing the manuscript. All authors discussed the results and commented on the manuscript.

Competing interests. The authors declare no competing interests.

Additional information

Supplementary information is available for this paper at https:

Correspondence and requests for materials should be addressed to D. G. Zhang

Reprints and permissions information is available at www.nature.com/rep

References

1. Murphy DB. *Fundamentals of Light Microscopy and Electronic Imaging 2nd edn*. Wiley-Blackwell (2013).

2. Diekmann R*, et al.* Chip-based wide field-of-view nanoscopy. *Nature Photonics* **11**, 322-328 (2017).

3. Helle ØI, Dullo FT, Lahrberg M, Tinguely J-C, Hellesø OG, Ahluwalia BS. Structured illumination microscopy using a photonic chip. *Nature Photonics* **14**, 431-438 (2020).

4. Ruh D, Mutschler J, Michelbach M, Rohrbach A. Superior contrast and resolution by image formation in rotating coherent scattering (ROCS) microscopy. *Optica* **5**, 1371-1381 (2018).

5. Fahrbach FO, Rohrbach A. Propagation stability of self-reconstructing Bessel beams enables contrast-enhanced imaging in thick media. *Nature Communications* **3**, 632 (2012).

6. Kudo S, Magariyama Y, Aizawa SI. Abrupt changes in flagellar rotation observed by laser dark-field microscopy. *Nature* **346**, 677-680 (1990).

7. Yasuda R, Noji H, Yoshida M, Kinosita K, Itoh H. Resolution of distinct rotational substeps by submillisecond kinetic analysis of F-1-ATPase. *Nature* **410**, 898-904 (2001).

8. Nishiyama M, Muto E, Inoue Y, Yanagida T, Higuchi H. Substeps within the 8-nm step of the ATPase cycle of single kinesin molecules. *Nature Cell Biology* **3**, 425-428 (2001).

9. Horio T, Hotani H. Visualization of the dynamic instability of individual microtubules by dark-field microscopy. *Nature* **321**, 605-607 (1986).

10. Gage SH. Modern Dark-Field Microscopy and the History of Its Development. *Transactions of the American Microscopical Society* **39**, 95-141 (1920).

11. Hecht E. *Optics 3rd edn*. Addison-Wesley (1998).

12. Kwon H, Arbabi E, Kamali SM, Faraji-Dana M, Faraon A. Single-shot quantitative phase gradient microscopy using a system of multifunctional metasurfaces. *Nature Photonics* **14**, 109-114 (2020).

13. Balaur E*, et al.* Plasmon-induced enhancement of ptychographic phase microscopy via sub-surface nanoaperture arrays. *Nature Photonics* **15**, 222-229 (2021).

14. Chazot CAC*, et al.* Luminescent surfaces with tailored angular emission for compact dark-field imaging devices. *Nature Photonics* **14**, 310-315 (2020).

15. Kats MA. Dark field on a chip. *Nature Photonics* **14**, 266-267 (2020).

16. von Olshausen P, Rohrbach A. Coherent total internal reflection dark-field microscopy: label-free imaging beyond the diffraction limit. *Optics Letters* **38**, 4066-4069 (2013).

17. Kim S, Blainey PC, Schroeder CM, Xie XS. Multiplexed single-molecule assay for enzymatic activity on flow-stretched DNA. *Nature Methods* **4**, 397-399 (2007).

18. Yeh P, Yariv A, Hong CS. Electromagnetic Propagation in Periodic Stratified Media .1. General Theory. *Journal of the Optical Society of America* **67**, 423-438 (1977).

19. Joannopoulos J, Johnson S, Winn J, Meade R. *Photonic Crystals: Molding the Flow of Light - Second Edition* (2011).

20. Anemogiannis E, Glytsis EN, Gaylord TK. Determination of guided and leaky modes in lossless and lossy planar multilayer optical waveguides: Reflection pole method and wavevector density method. *J Lightwave Technol* **17**, 929-941 (1999).

21. Hu H, Ma C, Liu Z. Plasmonic dark field microscopy. *Applied Physics Letters* **96**, 113107-113103 (2010).

22. Zhang D*, et al.* Back focal plane imaging of directional emission from dye molecules coupled to one-dimensional photonic crystals. *Nanotechnology* **25**, 145202 (2014).

23. Hassan K*, et al.* Momentum-space spectroscopy for advanced analysis of dielectric-loaded surface plasmon polariton coupled and bent waveguides. *Physical Review B* **87**, 195428 (2013).

24. Born M, Wolf E. *Principles of optics : electromagnetic theory of propagation, interference and diffraction of light 7th edn*. Cambridge Univ.Press, (1999).

25. Sinibaldi A*, et al.* Direct comparison of the performance of Bloch surface wave and surface plasmon polariton sensors. *Sensors and Actuators B: Chemical* **174**, 292-298 (2012).

26. Maier S. *Plasmonics: Fundamentals and Applications* (2007).

27. Axelrod D, Thompson N, Burghardt T. Total internal reflection fluorescent microscopy. *Journal of microscopy* **129**, 19-28 (1983).

28. Wang W*, et al.* Label-free measuring and mapping of binding kinetics of membrane proteins in single living cells. *Nature Chemistry* **4**, 846-853 (2012).

29. Ortega Arroyo J, Cole D, Kukura P. Interferometric scattering microscopy and its combination with single-molecule fluorescence imaging. *Nature Protocols* **11**, 617-633 (2016).

30. Arroyo JO, Kukura P. Non-fluorescent schemes for single-molecule detection, imaging and spectroscopy. *Nature Photonics* **10**, 11-17 (2016).

Figures

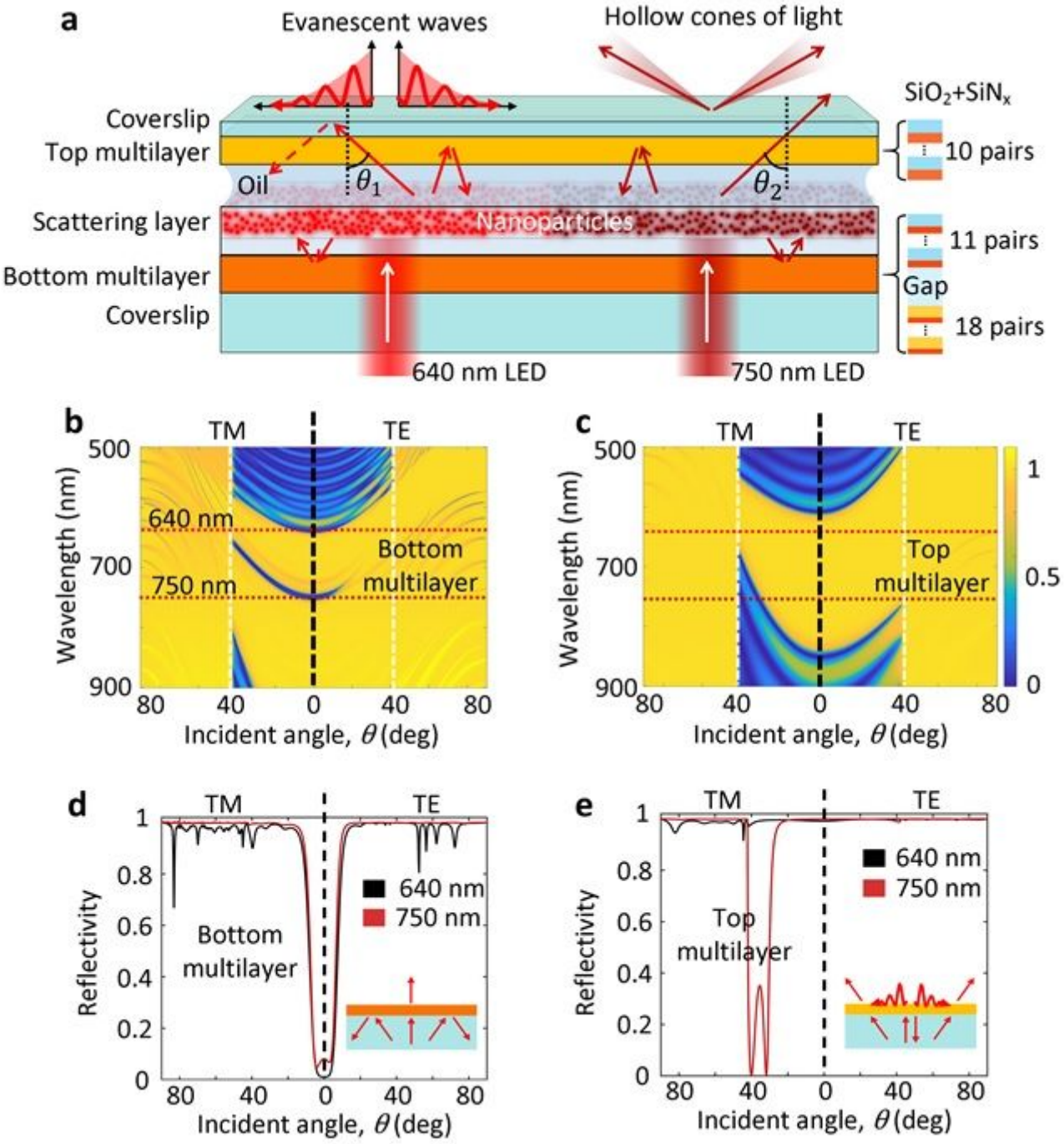

Figure 1

Schematic of the planar photonics chip and its photonic band gaps. (a) The photonic chips composed of three parts, the bottom (29 pairs of SiO2+SiNx in total), top multilayer (10 pairs of SiO2+SiNx in total), and the scattering layer (doped with TiO2 nanoparticles). Under normal incidence of 640 nm or 750 nm wavelength light, evanescent wavs or hollow cones of light can be generated at the top surface, respectively. (b) and (c) Calculated PBGs of the bottom and top multilayers. The horizontal red-dashed lines represent the positions of the incident wavelengths, 640 and 750 nm. The vertical white-dashed lines represent the position of the TIR angle at glass/air interface (corresponding to N.A =1). The left parts of the (b) and (c) are of the TM -polarized incident beam and the right parts TE-polarized one,

separated by the vertical black-dashed lines. (d) and (e) Calculated angular-dependent reflectivity of the bottom and top multilayers. The incident wavelengths are set as 640 and 750 nm. The incident polarization is of either TM (left part) or TE (right part). The insets on (d) and (e) simply presents the designed roles of the bottom and top multilayers.

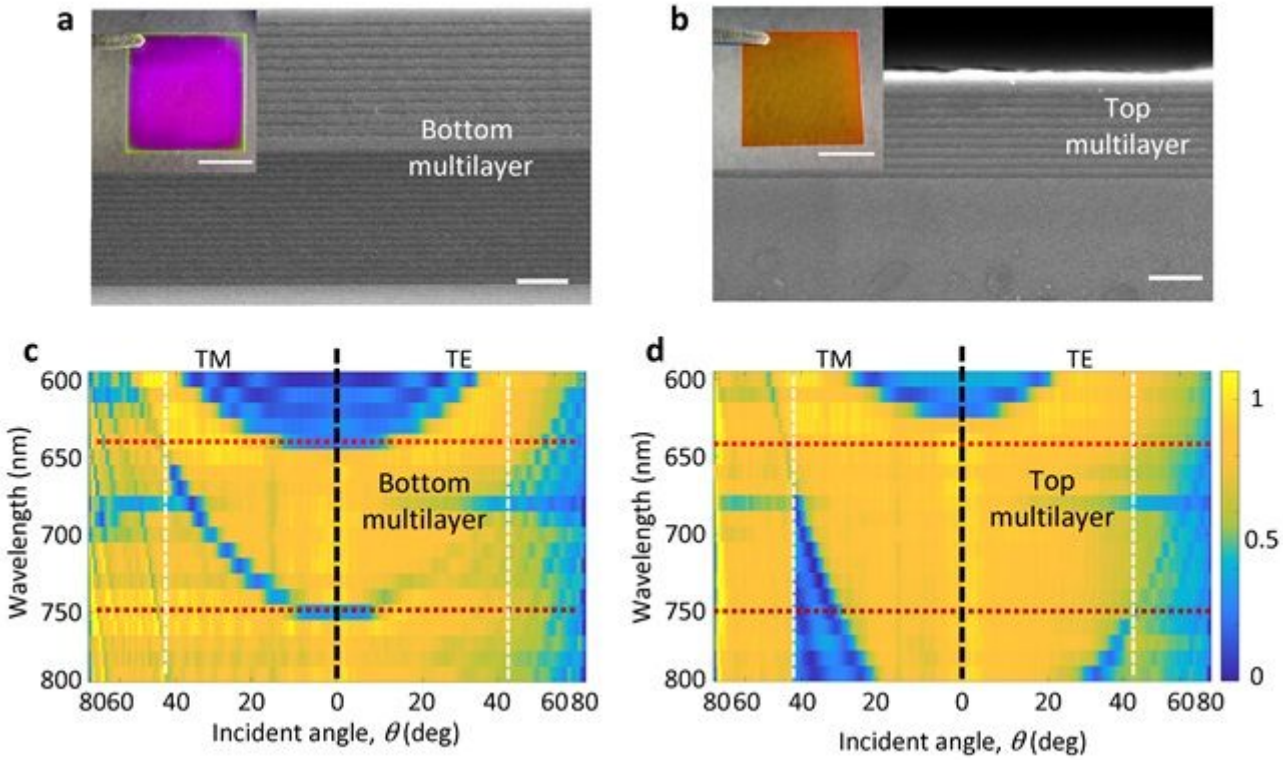

Figure 2

The fabricated bottom and top multilayers and their BFP imaging characterizations. (a) and (b) Cross-sectional SEM view of bottom and top multilayers. Scale bar, 1 μm. The insets on (a) and (b) are the photos of the multilayers fabricated on a coverslip, respectively. Scale bar, 1 cm. (c) and (d) Measured PBGs of the bottom and top multilayer with the reflective BFP imaging setup. The left parts are of the TM -polarized incident beam and the right parts TE-polarized one, separated by the vertical black-dashed lines. The horizontal red-dashed lines represent the positions of the incident wavelengths, 640 nm and 750 nm. The vertical white-dashed lines represent the position of the TIR angle at glass/air interface, corresponding to the N. A= 1.

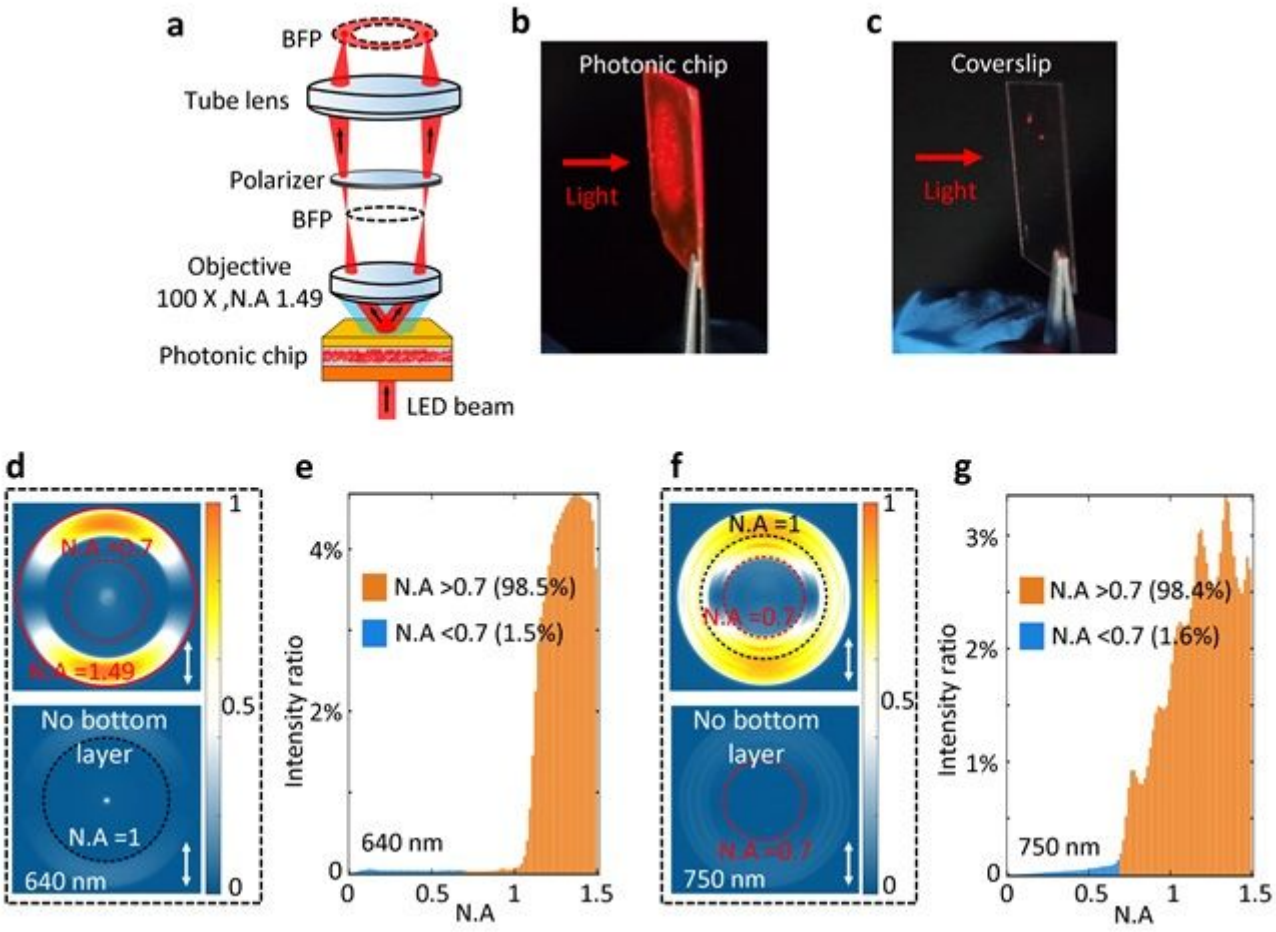

Figure 3

Measuring the transmissive directions of the scattered light from the photonic chip. (a) Schematic of the experimental setup for the transmissive BFP imaging. (b) and (c) The photos of the photonic chip and a coverslip when a light beam passes through, which show that light filed can be generated at the surface of the photonic chip. (d) and (f) transmission BFP images of the photonic chip under normal incidence with a LED beam, the incident wavelengths are selected as 640 and 750 nm. The bottom panels of (d) and (f) are the case where the bottom multilayer of the photonic chip was removed, to demonstrate the role of bottom multilayer. Comparisons between top and bottom panels of (d) and (f) shows that the bottom multilayer can amplify the intensity of the transmissive light from the photonic chip. The red-dashed circle represents the position with N.A =0.7 (for a regular air objective used in the darkfield and TIR imaging experiments) and the black one N.A =1 (corresponding to the TIR angle), the oil-immersed objective's numerical aperture is marked with a red-solid circle (N. A=1.49). The orientation of the polarizer is marked with a solid arrow on (d) and (f). (e) and (g) Quantitatively demonstrating the angular distribution of the transmissive light from the photonic chip. The N.A of the horizontal axis is corresponding to transmission angle θ (N.A =n* sin(θ), n is the refractive of the oil). The intensity of the transmissive light within low N.A (< 0.7) is about 1.5% (or 1.6 %), meaning that the direct transmission of the scattering light from the photonic chip is very weak.

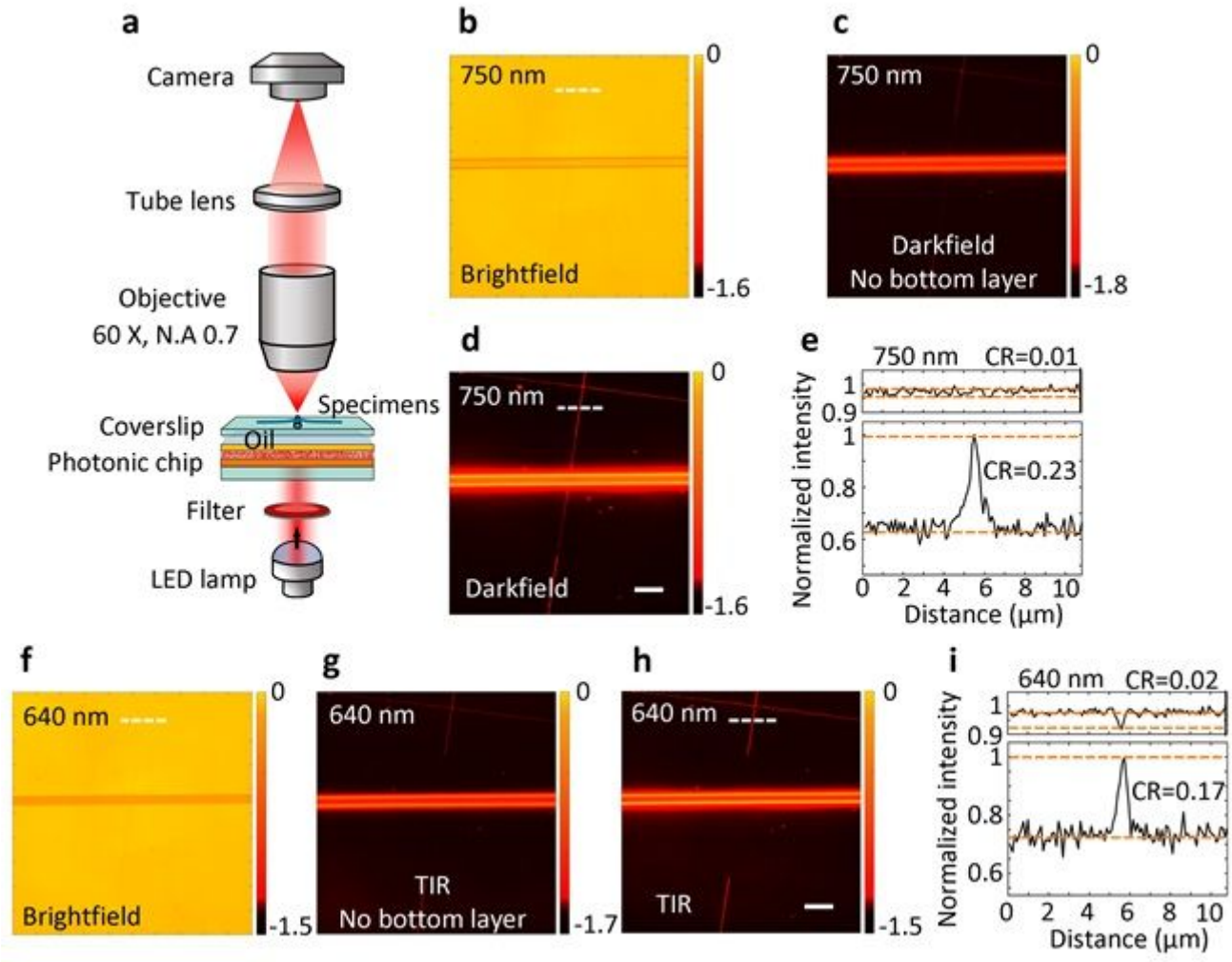

Figure 4

C-DFM and C-TIRM enabled by the photonic chip installed on a conventional brightfield microscopy. (a) Schematic of the brightfield microscopy with the photonic chip. The specimen to be imaged is a polymer nanowire placed on a polymer microwire (insets of (b) and (f)). (b) and (f) the brightfield images of the specimens, when they were placed on a bare coverslip. (c) and (d) C-DFM images, (g) and (h) C-TIRM images. For (c) and (g), the bottom multilayer of the photonic chip was removed, to demonstrate the role of the bottom multilayer in the C-DFM and C-TIRM. (e) Intensity profiles extracted along the white dashed lines on (b) and (d), (i) Intensity profiles extracted from (f) and (h). The red lines indicate the levels used to determine the image contrasts (CR). From (b) to (e), the incident wavelength is 750 nm, and from (f) to (i), the wavelength is 640 nm. Scale bars, 20μm.

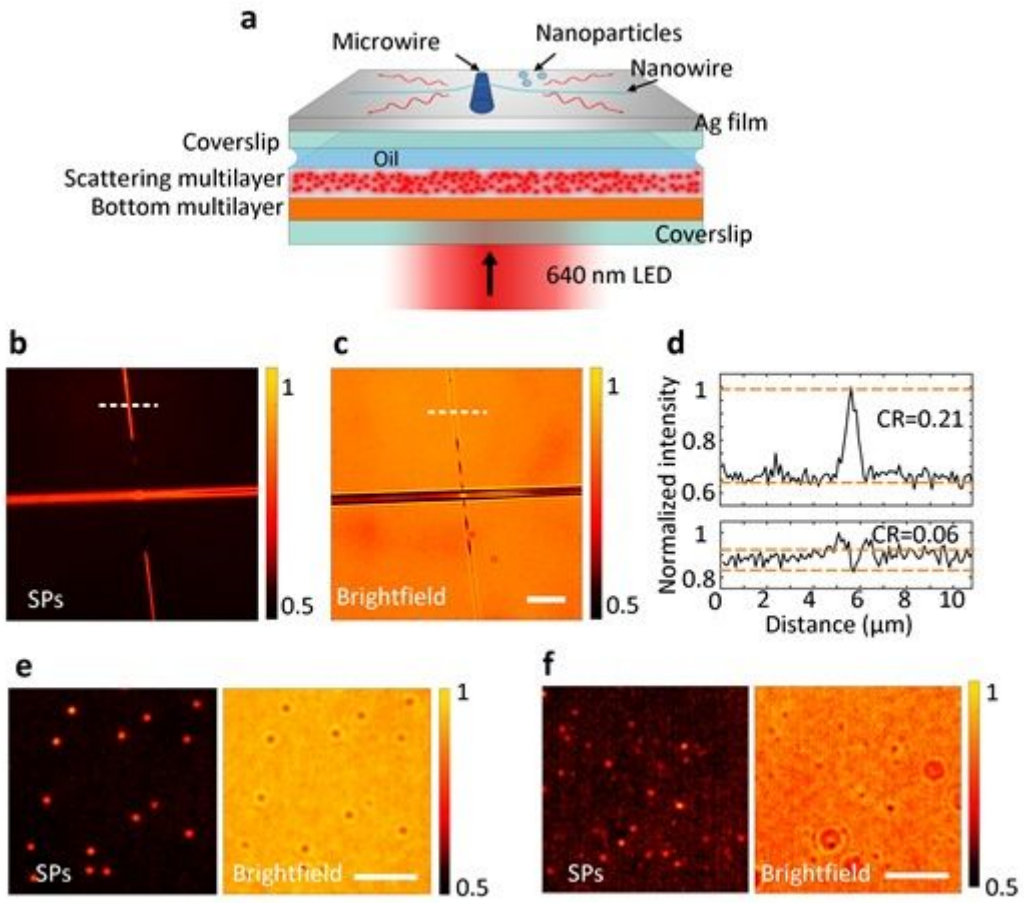

Figure 5

Excitations of SPs with the photonic chip for surface-imaging. (a) Schematic of the modified photonic chip where the top multilayer was replaced with a thin silver film to demonstrate the excitation of SPs under normal incidence and the ability for surface-imaging. The specimens to be imaged are the single polymer nanowire placed on a microwire, and polymer nanoparticles of different diameters. The modified photonic chip was also used in the standard brightfield microscopy as shown in Figure 4(a). (b) the image of the polymer wires under the illuminations of the excited SPs. (c) corresponding brightfield image of the polymer wires. (d) Intensity profiles extracted along the white dashed lines on (b) and (c). The dashed red lines indicate the levels used to determine the image contrasts (CR). (e), (f) The surface-images and brightfield images of the polymer nanoparticles with diameter at 200 nm and 50 nm, respectively. Scale bars, 10 μm.

Supplementary Files

This is a list of supplementary files associated with this preprint. Click to download.

- Supplementaryinformation.docx